Supplement of Atmos. Chem. Phys., 24, 14177–14190, 2024
https://doi.org/10.5194/acp-24-14177-2024-supplement

Atmospheric Chemistry and Physics
Open Access
EGU

Supplement of

Heterogeneous formation and light absorption of secondary organic aerosols from acetone photochemical reactions: remarkably enhancing effects of seeds and ammonia

Si Zhang et al.

Correspondence to: Gehui Wang (ghwang@geo.ecnu.edu.cn)

Supporting Information

This PDF file includes:

1. Supplementary Text S1-S5
2. Ten figures, Figure S1-S12
3. Three tables, Table S1-S3
4. References

Text S1. Particle wall loss correction

The particle wall loss was corrected by using a total-mass-concentration-based method (Liu and Abbatt, 2021). The wall-loss-corrected sulfate concentration at time t $wC_{so_4^{2-}}(t)$ can be calculated using the Eq.(1).

$$wC_{so_4^{2-}}(t) = C^{sus}_{so_4^{2-}}(t) + k\int_0^t C^{sus}_{so_4^{2-}}(t)dt \quad (1)$$

where $C^{sus}_{so_4^{2-}}(t)$ is the measured sulfate concentration at time t, and k is the first order particles wall loss rate constant, 1×10^{-4} s^{-1} in this study. The wall loss rate constants of pure $(NH_4)_2SO_4$ seed and NH_4NO_3 seed were similar under the experimental conditions in this work.

Text S2. NH_3 concentration wall loss correction

According to the reports of Huang et al. (2018)and Zhang et al. (2014), the vapor wall loss of gas compounds in Teflon-walled chambers can be estimated by a two-layer model, and the overall mass transport coefficient across the gas-phase boundary layer and the air-Teflon interface can be calculated by Eq.2-4. Then the first-order wall loss coefficient (k_w) can be calculated by Eq.5. Therefore, the loss of NH_3 to the chamber wall is estimated by the k_w by considering the gas-phase transport within the chamber, as reported by Zhang et al. (2014)

$$v_1 = \left(\frac{1}{v_e} + \frac{1}{v_c}\right)^{-1} \quad (2)$$

$$v_e = \frac{2}{\pi}\sqrt{k_e \mathcal{D}_g} \quad (3)$$

$$v_c = \frac{\alpha_w \omega}{4} \quad (4)$$

$$k_w = \left(\frac{A}{V}\right)v_1 = \left(\frac{A}{V}\right)\frac{\alpha_w \omega}{4 + \frac{\pi}{2}\left(\frac{\alpha_w \omega}{\sqrt{k_e D_g}}\right)} \quad (5)$$

where A/V is the surface-to-volume ratio of the chamber; α_w is the mass accommodation coefficient of NH_3 onto the Teflon chamber walls at RH = 90% (0.01) (Bongartz et al., 1995); ω is the mean molecular speed of NH_3 (603 m s^{-1}) (Seinfeld and Pandis, 2006); k_e is the

coefficient of eddy diffusion and is estimated to be 0.31 for the chamber used in this work; D_g is the gas-phase diffusion coefficient (1.98×10^{-5}) (Tang et al., 2014).

Therefore, the loss of NH_3 to the chamber wall is estimated by the k_w by considering the gas-phase transport within the chamber (Zhang et al., 2014). The average concentration of NH_3 is estimated by eq. 6,

$$[\overline{NH_3}]=\frac{1-e^{-k_w\Delta t}}{k_w\Delta t}[NH_3]_0 \quad (6)$$

where the first-order wall-loss coefficient (k_w) of NH_3 in this study is 9.5×10^{-3} s^{-1} and Δt is the reaction time. For an initial injection concentration of 1250 ppbv NH_3, the average concentration of NH_3 in the chamber was corrected to be 73 ppbv.

Text S3. VOCs concentration wall loss correction and estimation of MGly concentration

The vapor wall loss coefficients of VOCs in chamber were also calculated by Eq.2. The values of α_w, k_e, ω and D_g of VOCs were calculated by eq.7-10, respectively (Huang et al., 2018).

$$\alpha_w = 10^{-2.744}(c^*)^{-0.6566} \quad (7)$$

$$\log_{10}c^* = (n_C^0 - n_C)b_C - n_O b_O - 2\frac{n_C n_O}{n_C + n_O}b_{CO} - n_N b_N - n_S b_S, \quad (8)$$

$$k_e = 0.004 + 10^{-2.25}(V)^{0.74} \quad (9)$$

$$\omega = \sqrt{\frac{8RT}{\pi MW_{voc}}} \quad (10)$$

where c^* is the vapor saturation concentration of VOCs, and the calculation method and all parameters were explained in detail by Li et al. (2016); R is the gas constant, 8.314 (kg m^2 s^{-2} K^{-1} mol^{-1}); T is the temperature; MW_{voc} is the vapor molecular weight of VOCs; D_g of VOCs were referred to the results of Tang et al. (2015).

In this study, the concentrations of MGly measured by PTR-MS were the equilibrium concentrations after gas-particle partitioning and multiphase reactions, which would underestimate the contribution of MGLY in the SOA formation. Hence, the total

concentrations of MGly in gas phase were estimated through the molar yield (14%) of MGLY in acetone-OH oxidation reported by Fu et al. (2008). Then the total concentrations of MGly were vapor wall loss corrected by k_w.

Text S4. The calculation of the MAC of SOA

In this study, the light absorption coefficient (Abs_λ, M m^{-1}) and the mass absorption coefficient (MAC_λ, m^2 g^{-1}) at the wavelength of λ of SOA were calculated using eq.13 and 14, respectively (Liu et al., 2023).

$$\mathrm{Abs}_\lambda = (A_\lambda - A_{700})\frac{V_w}{V_a \times l} \times \ln(10) \quad (13)$$

$$\mathrm{MAC}_\lambda = \frac{\mathrm{Abs}_\lambda}{M} \quad (14)$$

where A_λ and A_{700} represent the light absorption at the wavelengths of λ and 700 nm measured by LWCC, respectively; V_w and V_a represent the volume of solvent and the volume of air corresponding to the filter punch, respectively; and l is the absorbing path length (1 m); M is the concentration of water-soluble organic carbon (WSOC, μgC m^{-3}).

Text S5. The calculation of the partition coefficients of NH_3 ($\varepsilon(NH_4^+)$)

The partition coefficients of NH_3 ($\varepsilon(NH_4^+)$) on different seeds were calculated by eq.15 and 16 (Guo et al., 2017; Nah et al., 2018).

$$\varepsilon(NH_4^+) \cong \frac{\frac{\gamma_{H^+}10^{-pH}}{\gamma_{NH_4^+}} H^*_{NH_3} W_i RT \times 0.987 \times 10^{-14}}{1 + \frac{\gamma_{H^+}10^{-pH}}{\gamma_{NH_4^+}} H^*_{NH_3} W_i RT \times 0.987 \times 10^{-14}} \quad (15)$$

$$\ln(H^*_{NH_3}) = 25.393 - 10373.6(1/T_r - 1/T) + 4.131(T_r/T - (1 + \ln(T_r/T))) \quad (16)$$

where γ_{H^+} and $\gamma_{NH_4^+}$ are activity coefficients of H^+ and NH_4^+, respectively, calculated from E-AIM model; $H^*_{NH_3}$ is equilibrium constants calculated by eq.16; R is the gas constant; T is temperature; W_i is particle liquid water content associated with inorganic species.

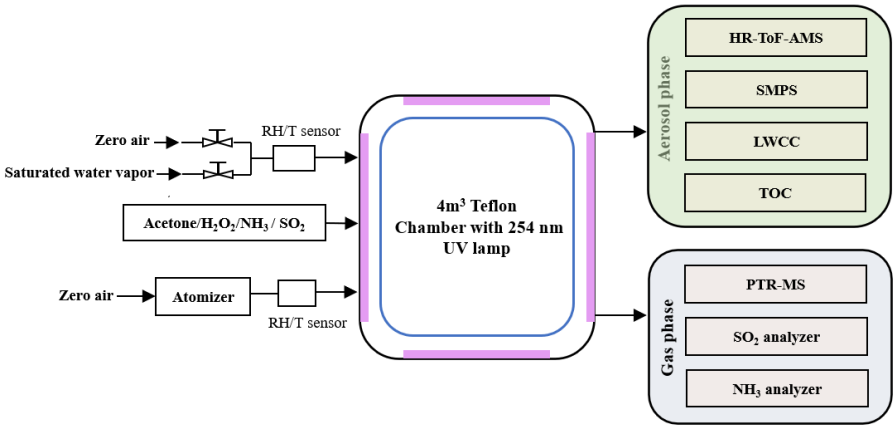

70

71 **Figure S1.** A schematic diagram of experimental setup in this work

72

73

74

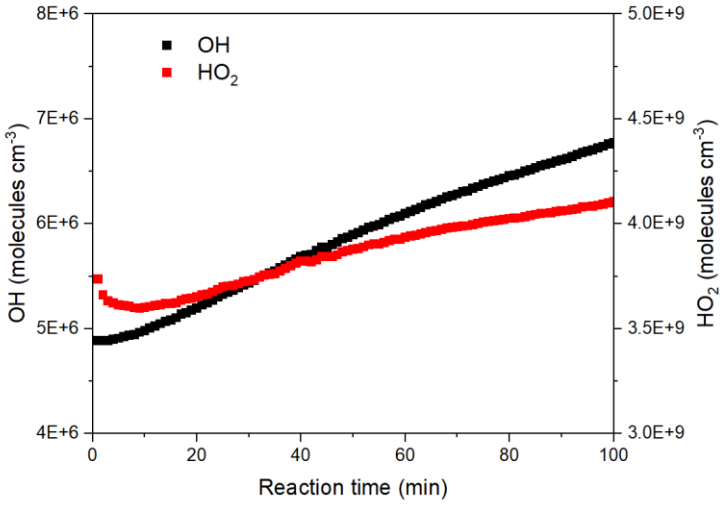

75

76 **Figure S2.** The times series of OH and HO_2 radical concentrations during Phase I.

77

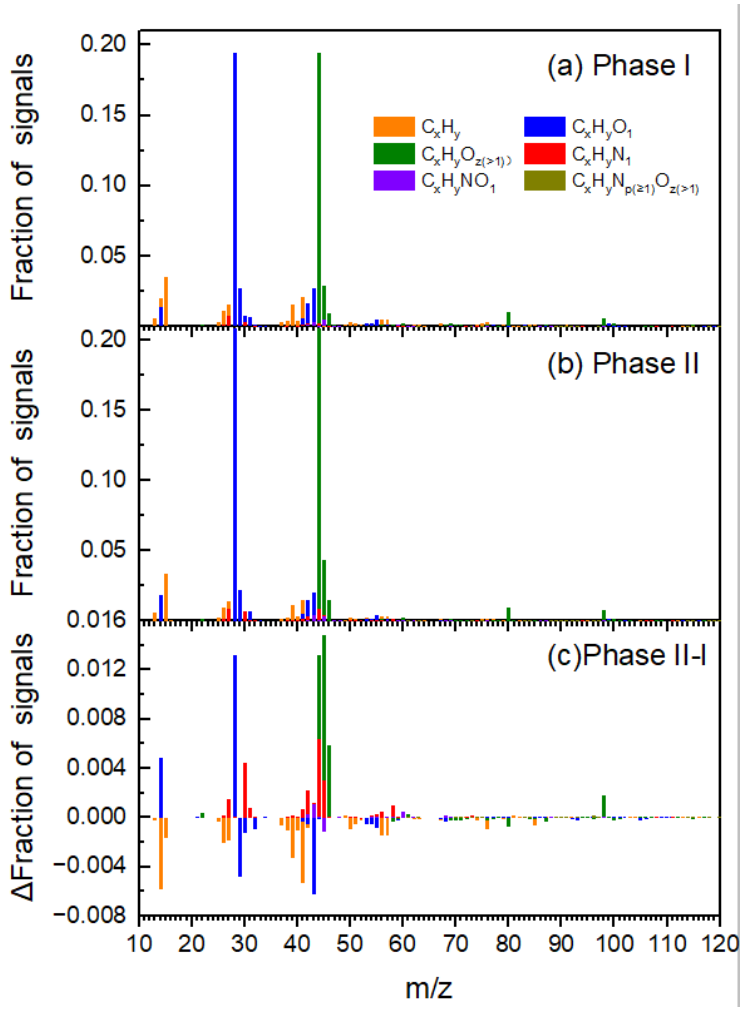

Figure S3. The mass spectra of acetone-derived SOA measured by HR-AMS during the Phase I and Phase II (a and b) and their difference between the two phases (c). Data were taken and analyzed at a high resolution but were summarized to a unit mass resolution for display.

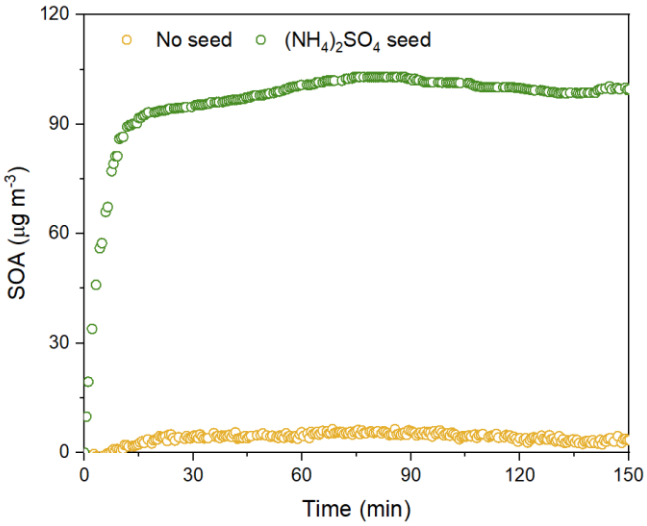

Figure S4. Concentrations of acetone-derived SOA in the chamber during the Phase I as a function of reaction time in the absence and presence of $(NH_4)_2SO_4$ seeds, respectively.

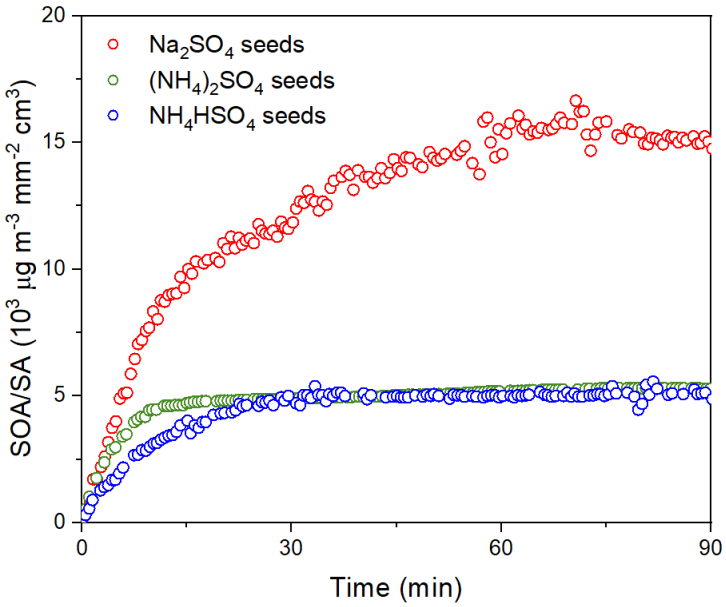

Figure S5. Normalized concentrations of SOA to the surface area (SA) of different seeds at Phase I as a function of reaction time during the exposure of various seeds to 750 ppb acetone and 5.3×10^8 molecules cm^{-3} OH radicals under 85% RH.

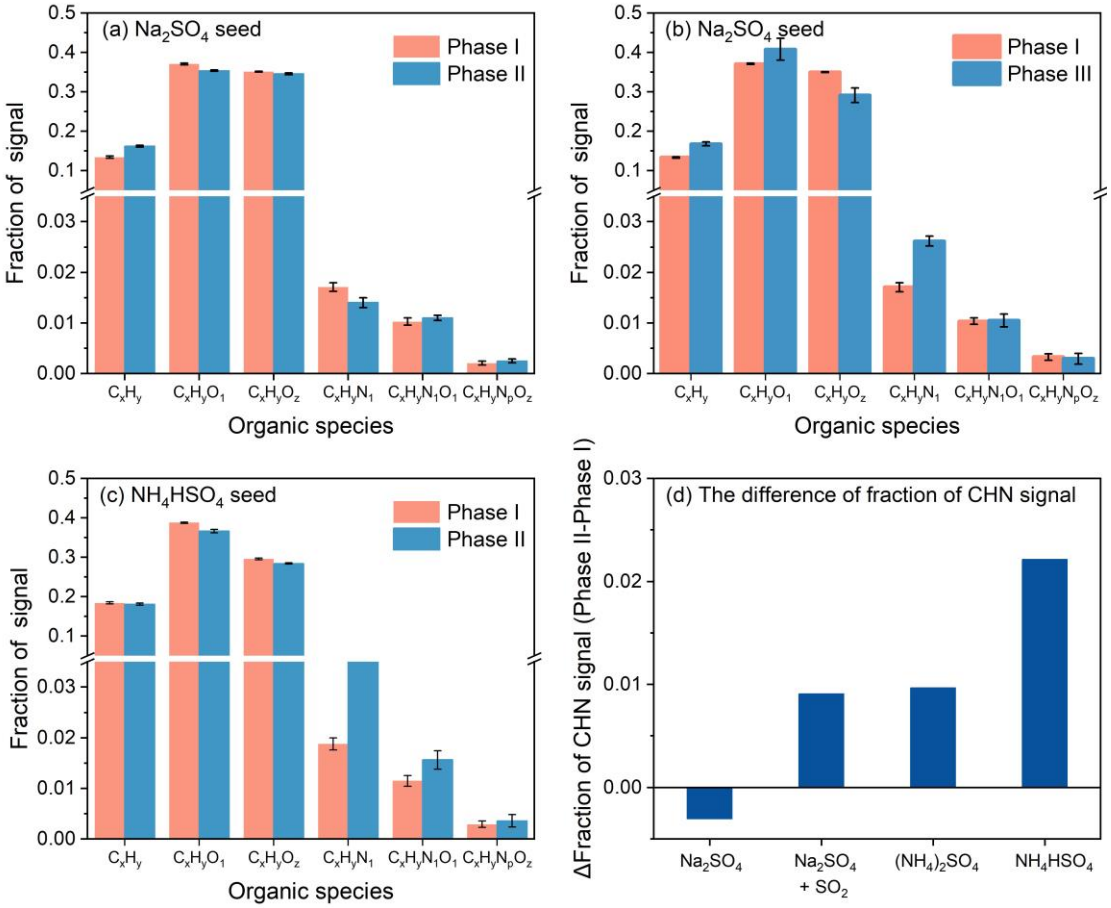

Figure S6. (a-c) The fraction of various organic species family signal of acetone-derived SOA at different reaction phases. (Phase I: Photoreaction of acetone by OH radicals without NH_3; Phase II: Reaction of acetone oxidation products with NH_3 under dark conditions; Phase III: Addition of 500 ppb SO_2 into the chamber after Phase II in the presence of Na_2SO_4 seeds); (d) The enhancement of the fraction of CHN ions family of Phase II over Phase I on different seeds (the value on Na_2SO_4 seed with SO_2 is the enhancement of Phase III over Phase I).

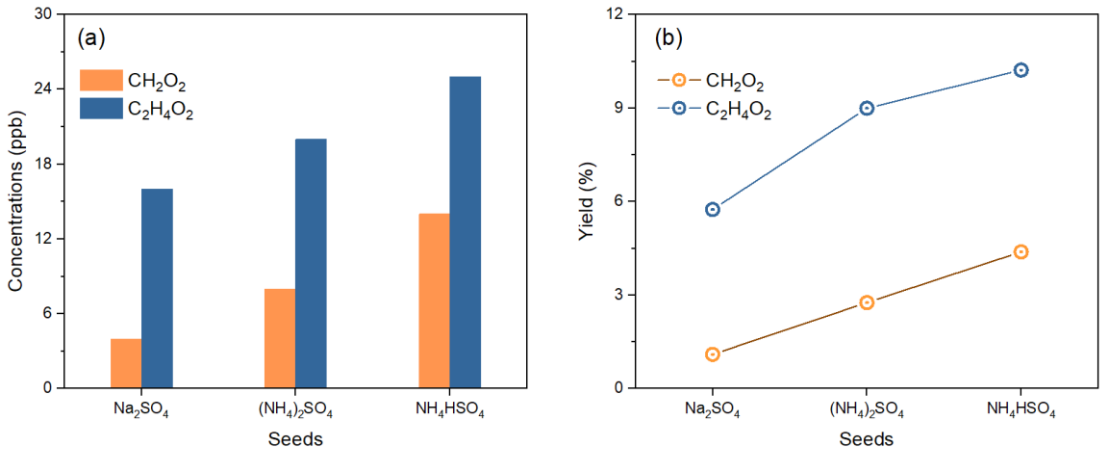

Figure S7. The concentrations (a) and yield (b) of formic and acetic acids in gas phase during steady state of reaction on various seeds.

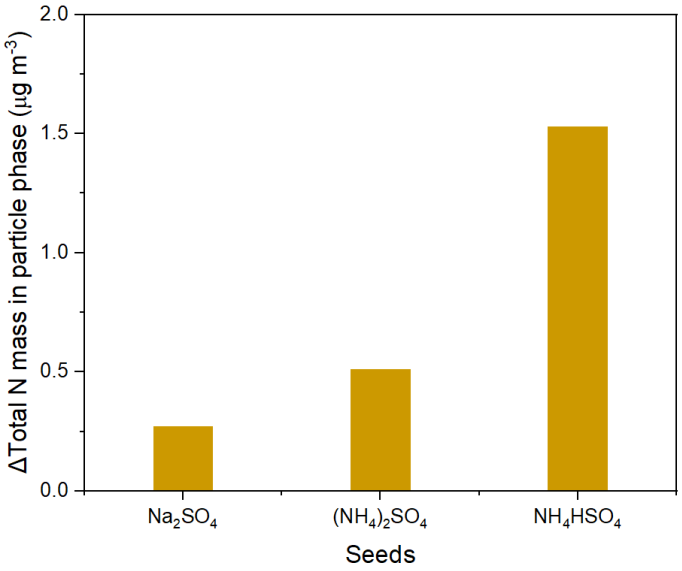

Figure S8. The enhancement of the total N mass in particle phase at Phase II.

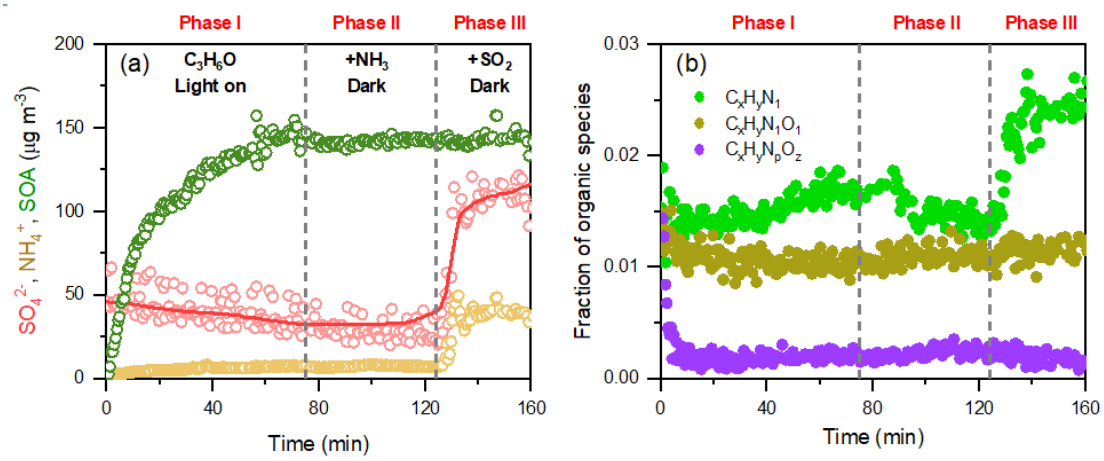

Figure S9. (a) The mass concentration of SOA, NH_4^+ and SO_4^{2-} during the reaction given by HR-ToF-AMS, which were corrected according to the results of SMPS; (b) The variations of fractions of N-containing organic species signals during the reaction on Na_2SO_4 seed with NH_3 and SO_2.

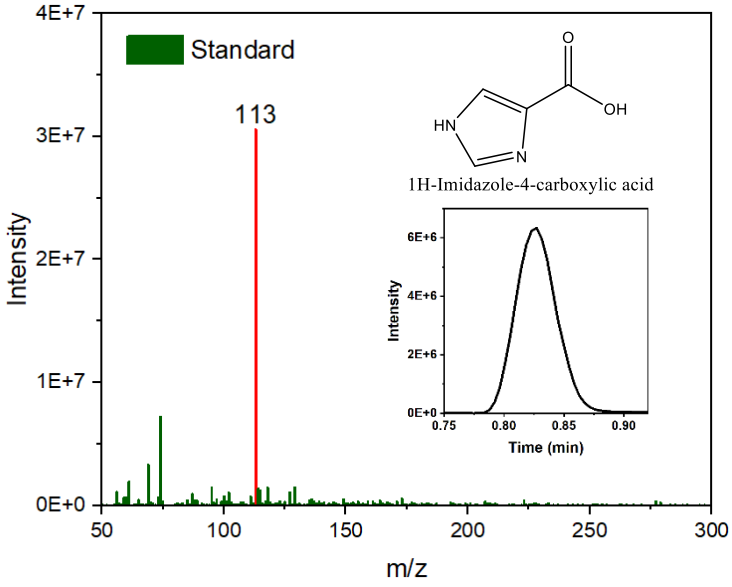

Figure S10. The ESI-Orbitrap MS spectra of the 1H-Imidazole-4-carboxylic acid standard.

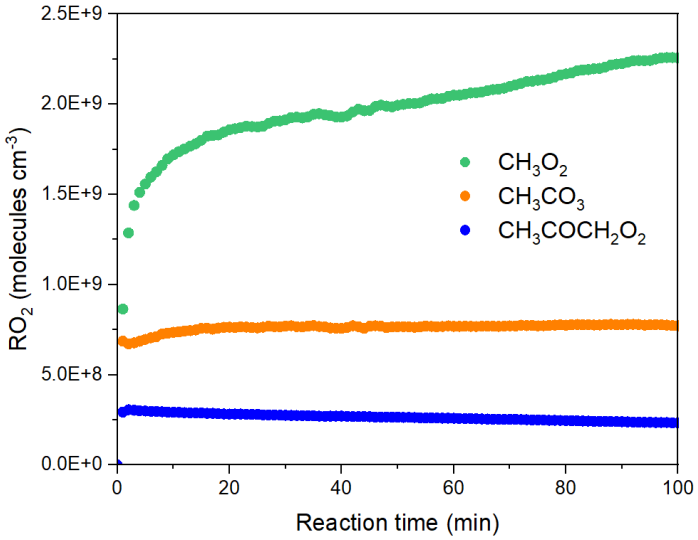

149

150 **Figure S11.** The times series of three main RO_2 concentrations during Phase I.

151

152

153

154

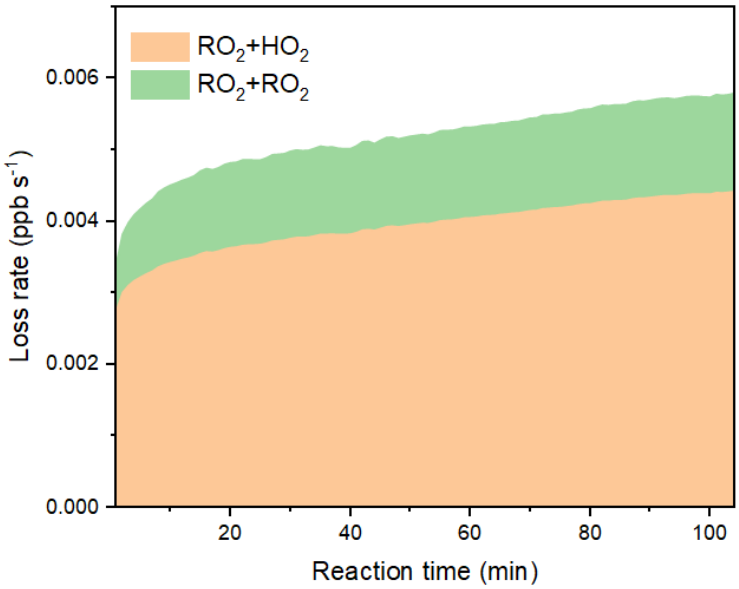

155

156 **Figure S12.** Loss rates of RO_2+HO_2 and RO_2+RO_2 pathways in acetone photoreaction
157 during the experiment

158 **Table S1.** The reaction conditions of the experiments

Exp. No.	Acetone (ppb)	OH[a] (molecules cm^{-3})	NH_3[b] (ppb)	SO_2 (ppb)	Seeds	RH (%)
1	750	5.89×10^6	73	/	$(NH_4)_2SO_4$	85±1
2	750	5.89×10^6	73	/	$(NH_4)HSO_4$	85±1
3	750	5.89×10^6	73	/	Na_2SO_4	85±1
4	750	5.89×10^6	73	500	Na_2SO_4	85±1
5	750	5.89×10^6	73	/	/	85±1

[a] The concentrations of OH radicals in all experiments are average concentrations during Phase I. These concentrations are determined using an OBM-MCM.

[b] The concentrations of NH_3 are wall-loss corrected average concentrations during Phase II, without considering the reaction process.

159

160

161

162 **Table S2.** ESI-Orbitrap MS measured products in acetone SOA

Measured Mass $[M+H]^+$	Theory Mass	Suggested Formula	Molecular Structure	Seeds	Ref.
72	71	C_3H_5NO	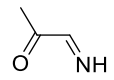		De Haan et al. (2019)
117	116	$C_5H_8O_3$	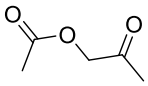		
133	132	$C_5H_8O_4$	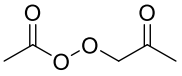		
163	162	$C_6H_{10}O_5$	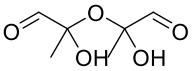	$(NH_4)_2SO_4$	Li et al. (2021b)
195	194	$C_9H_{10}N_2O_3$	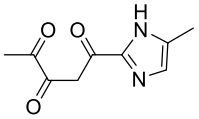		Aiona et al. (2017)
235	234	$C_9H_{14}O_7$	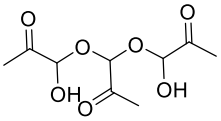		Li et al. (2021b)
341	340	$C_{15}H_{20}O_7N_2$	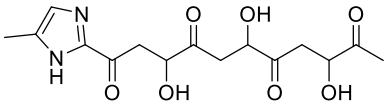		Aiona et al. (2017)
105	104	$C_3H_4O_4$	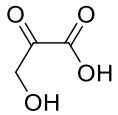		Altieri et al. (2008)
119	118	$C_4H_6O_4$	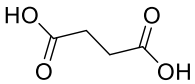		Altieri et al. (2008)
135	134	$C_4H_6O_5$	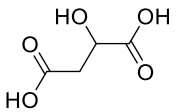		Altieri et al. (2008)
161	160	$C_6H_8O_5$	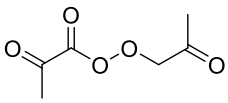	Na_2SO_4	
179	178	$C_6H_{10}O_6$	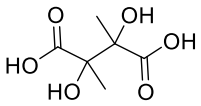		Guzmán et al. (2006)
217	216	$C_9H_{12}O_6$	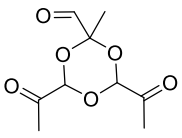		Zhao et al. (2006)

233	232	$C_9H_{12}O_7$	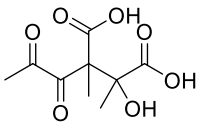	Tan et al. (2012)

Table S3 The concentrations and saturation mass concentration of VOCs products formed from acetone photooxidation in gas phase

Gaseous products	Molecular structure	Concentration (ppb)	C* (ug m^{-3})	Volatility	K_H (M atm^{-1})
$C_3H_4O_2$	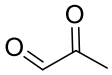	1.82	2.3×10^7	VOC	3.7×10^3
$C_2H_4O_2$	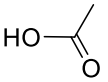	22.95	3.2×10^7	VOC	1.8×10^3
CH_2O_2	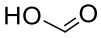	7.84	2.7×10^7	VOC	1.3×10^3
$C_2H_4O_3$	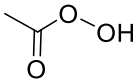	4.16	**1.4×10^6**	**IVOC**	7.2×10^2
CH_4O_2		7.95	2.7×10^7	VOC	1.5×10^2
CH_4O		0.35	6.7×10^8	VOC	2.3×10^2
$C_3H_6O_3$	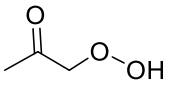	1.65	**1.5×10^6**	**IVOC**	3.1×10^4
$C_3H_6O_2$	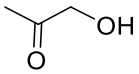	0.12	2.3×10^7	VOC	1.3×10^2

Reference:

Aiona, P. K., Lee, H. J., Leslie, R., Lin, P., Laskin, A., Laskin, J., and Nizkorodov, S. A.: Photochemistry of products of the aqueous reaction of methylglyoxal with ammonium sulfate, ACS Earth Space Chem., 1, 522-532, 10.1021/acsearthspacechem.7b00075, 2017.

Altieri, K. E., Seitzinger, S. P., Carlton, A. G., Turpin, B. J., Klein, G. C., and Marshall, A. G.: Oligomers formed through in-cloud methylglyoxal reactions: Chemical composition, properties, and mechanisms investigated by ultra-high resolution FT-ICR mass spectrometry, Atmospheric Environment, 42, 1476-1490, 10.1016/j.atmosenv.2007.11.015, 2008.

Bongartz, A., Schweighoefer, S., Roose, C., and Schurath, U.: The mass accommodation coefficient of ammonia on water, Journal of Atmospheric Chemistry, 20, 35-58, 10.1007/bf01099917, 1995.

De Haan, D. O., Pajunoja, A., Hawkins, L. N., Welsh, H. G., Jimenez, N. G., De Loera, A., Zauscher, M., Andretta, A. D., Joyce, B. W., De Haan, A. C., Riva, M., Cui, T. Q., Surratt, J. D., Cazaunau, M., Formenti, P., Gratien, A., Pangui, E., and Doussin, J. F.: Methylamine's Effects on Methylglyoxal-Containing Aerosol: Chemical, Physical, and Optical Changes, Acs Earth and Space Chemistry, 3, 1706-1716, 10.1021/acsearthspacechem.9b00103, 2019.

Fu, T. M., Jacob, D. J., Wittrock, F., Burrows, J. P., Vrekoussis, M., and Henze, D. K.: Global budgets of atmospheric glyoxal and methylglyoxal, and implications for formation of secondary organic aerosols, J. Geophys. Res.: Atmos., 113, D15303, 10.1029/2007jd009505, 2008.

Guo, H., Liu, J., Froyd, K. D., Roberts, J. M., Veres, P. R., Hayes, P. L., Jimenez, J. L., Nenes, A., and Weber, R. J.: Fine particle pH and gas–particle phase partitioning of inorganic species in Pasadena, California, during the 2010 CalNex campaign, Atmos. Chem. Phys., 17, 5703-5719, 10.5194/acp-17-5703-2017, 2017.

Guzmán, M. I., Colussi, A. J., and Hoffmann, M. R.: Photoinduced Oligomerization of Aqueous Pyruvic Acid, The Journal of Physical Chemistry A, 110, 3619-3626, 10.1021/jp056097z, 2006.

Huang, Y., Zhao, R., Charan, S. M., Kenseth, C. M., Zhang, X., and Seinfeld, J. H.: Unified theory of vapor–wall mass transport in Teflon-walled environmental chambers, Environ. Sci. Technol., 52, 2134-2142, 10.1021/acs.est.7b05575, 2018.

Li, Y., Pöschl, U., and Shiraiwa, M.: Molecular corridors and parameterizations of volatility in the chemical evolution of organic aerosols, Atmospheric Chemistry and Physics, 16, 3327-3344, 10.5194/acp-16-3327-2016, 2016.

Li, Y. X., Zhao, J. Y., Wang, Y., Seinfeld, J. H., and Zhang, R. Y.: Multigeneration production of secondary organic aerosol from toluene photooxidation, Environ. Sci. Technol., 55, 8592-8603, 10.1021/acs.est.1c02026, 2021a.

Li, Y. X., Ji, Y. M., Zhao, J. Y., Wang, Y., Shi, Q. J., Peng, J. F., Wang, Y. Y., Wang, C. Y., Zhang, F., Wang, Y. X., Seinfeld, J. H., and Zhang, R. Y.: Unexpected oligomerization of small alpha-dicarbonyls for secondary organic aerosol and brown carbon formation, Environ. Sci. Technol., 55, 4430-4439, 10.1021/acs.est.0c08066, 2021b.

Liu, T. and Abbatt, J. P. D.: Oxidation of sulfur dioxide by nitrogen dioxide accelerated at the interface of deliquesced aerosol particles, Nat. Chem., 13, 1173–1177, 10.1038/s41557-021-00777-0, 2021.

Liu, X., Wang, H., Wang, F., Lv, S., Wu, C., Zhao, Y., Zhang, S., Liu, S., Xu, X., Lei, Y., and Wang, G.: Secondary formation of atmospheric brown carbon in China haze: Implication for an enhancing role of ammonia, Environ. Sci. Technol., 57, 11163-11172, 10.1021/acs.est.3c03948, 2023.

Nah, T., Guo, H., Sullivan, A. P., Chen, Y., Tanner, D. J., Nenes, A., Russell, A., Ng, N. L., Huey, L. G., and Weber, R. J.: Characterization of aerosol composition, aerosol acidity, and organic acid

partitioning at an agriculturally intensive rural southeastern US site, Atmospheric Chemistry and Physics, 18, 11471-11491, 10.5194/acp-18-11471-2018, 2018.

Seinfeld, J. H. and Pandis, S. N.: ATMOSPHERIC CHEMISTRY AND PHYSICS: from air pollution to climate change, John Wliey & Sons, 2nd ed., ISBN: 978-0-471-72018-8, 2006.

Tan, Y., Lim, Y. B., Altieri, K. E., Seitzinger, S. P., and Turpin, B. J.: Mechanisms leading to oligomers and SOA through aqueous photooxidation: insights from OH radical oxidation of acetic acid and methylglyoxal, Atmospheric Chemistry and Physics, 12, 801-813, 10.5194/acp-12-801-2012, 2012.

Tang, M. J., Cox, R. A., and Kalberer, M.: Compilation and evaluation of gas phase diffusion coefficients of reactive trace gases in the atmosphere: volume 1. Inorganic compounds, Atmospheric Chemistry and Physics, 14, 9233-9247, 10.5194/acp-14-9233-2014, 2014.

Tang, M. J., Shiraiwa, M., Pöschl, U., Cox, R. A., and Kalberer, M.: Compilation and evaluation of gas phase diffusion coefficients of reactive trace gases in the atmosphere: Volume 2. Diffusivities of organic compounds, pressure-normalised mean free paths, and average Knudsen numbers for gas uptake calculations, Atmospheric Chemistry and Physics, 15, 5585-5598, 10.5194/acp-15-5585-2015, 2015.

Zhang, X., Cappa, C. D., Jathar, S. H., McVay, R. C., Ensberg, J. J., Kleeman, M. J., and Seinfeld, J. H.: Influence of vapor wall loss in laboratory chambers on yields of secondary organic aerosol, Proc Natl Acad Sci U S A, 111, 5802-5807, 10.1073/pnas.1404727111, 2014.

Zhao, J., Levitt, N. P., Zhang, R. Y., and Chen, J. M.: Heterogeneous reactions of methylglyoxal in acidic media: Implications for secondary organic aerosol formation, Environmental Science & Technology, 40, 7682-7687, 10.1021/es060610k, 2006.